Season-dependent dynamics of nonlinear optimal error growth and El Niño-Southern Oscillation predictability in a theoretical model

Mu Mu,[1] Wansuo Duan,[1] and Bin Wang[2]

Received 13 December 2005; revised 9 January 2007; accepted 20 January 2007; published 24 May 2007.

[1] Most state-of-the-art climate models have difficulty in the prediction of El Niño-Southern Oscillation (ENSO) starting from preboreal spring seasons. The causes of this spring predictability barrier (SPB) remain elusive. With a theoretical ENSO system model, we investigate this controversial issue by tracing the evolution of conditional nonlinear optimal perturbation (CNOP) and by analyzing the behavior of initial error growth. The CNOPs are the errors in the initial states of ENSO events, which have the biggest impact on the uncertainties at the prediction time under proper physical constraints. We show that the evolution of CNOP-type errors associated with El Niño episodes depends remarkably on season with the fastest growth occurring during boreal spring in the onset phase. There also exist other kinds of initial errors, which have either somewhat smaller growth rates or neutral ones during spring. However, for La Niña events, even if initial errors are of CNOP-type, the errors grow without significant seasonal dependence. These findings suggest that the SPB in this model results from combined effects of three factors: the annual cycle of the mean state, the structure of El Niño, and the pattern of the initial errors. On the basis of the error tendency equations derived from the model, we addressed how the combination of the three factors causes the SPB and proposed a mechanism responsible for the error growth in the model ENSO events. Our results help in clarifying the role of the initial error pattern in SPB, which may provide a clue for explaining why SPB can be eliminated by improving initial conditions. The results also illustrate a theoretical basis for improving data assimilation in ENSO prediction.

Citation: Mu, M., W. Duan, and B. Wang (2007), Season-dependent dynamics of nonlinear optimal error growth and El Niño-Southern Oscillation predictability in a theoretical model, *J. Geophys. Res.*, *112*, D10113, doi:10.1029/2005JD006981.

1. Introduction

[2] Considerable effort has been invested in understanding and simulating the phenomenon of El Niño-Southern Oscillation (ENSO) by using models of varying complexity. These models range from theoretical ones [*Wang and Fang*, 1996; *Jin*, 1997a, 1997b; *Wang et al.*, 1999; *Wang*, 2001], through the so-called intermediate coupled model [*McCreary and Anderson*, 1991; *Cane et al.*, 1986; *Suarez and Schopf*, 1988; *Battisti and Hirst*, 1989; *Philander*, 1990; *McCreary and Anderson*, 1991; *Kleeman et al.*, 1995; *Picaut and Delcroix*, 1995; *Neelin et al.*, 1998], to complex coupled general circulation models (CGCMs). Both intermediate coupled models [e.g., *Zebiak and Cane*, 1987] and CGCMs have been used to forecast ENSO. Recently, the climate forecast system at the National Center for Environmental Prediction [*Saha et al.*, 2006], the seasonal forecast systems at the European Center for Medium-Range Weather Forecasts, and the Multimodel Ensemble System at EU [*Palmer et al.*, 2004] and at Asia-Pacific Economic Cooperation Climate Center have also been developed for seasonal to interannual climate prediction.

[3] A detailed comparison of ENSO models was given by *Kirtman et al.* [2002]. They indicated that it is difficult to tell which model shows higher forecast capability for the dynamical and statistical models or intermediate and complex models. To improve ENSO forecast skill, it is necessary to explore the fundamental physics of ENSO for which a theoretical model is useful. *Wang and Fang* [1996], *Jin* [1997a, 1997b], and others have developed analytical models to advance the understanding on ENSO physics and have obtained significant results.

[4] "Spring predictability barrier" (SPB) is a well-known characteristic of ENSO forecasts. The SPB is referred to a phenomenon that most ENSO prediction models often experience an apparent drop in prediction skill across April and May [*Webster and Yang*, 1992]. SPBs exist in coupled and statistical models. In some occasions, the SPB is even stronger in statistical models than in GCMs [*van Oldenborgh et al.*, 2005]. Many works have investigated this phenomenon [*Walker*, 1924; *Webster and Yang*, 1992; *Webster*, 1995;

[1]State Key Laboratory of Numerical Modeling for Atmospheric Sciences and Geophysical Fluid Dynamics, Institute of Atmospheric Physics, Chinese Academy of Sciences, Beijing, China.
[2]Department of Meteorology, School of Ocean and Earth Science and Technology, University of Hawaii, Honolulu, Hawaii, USA.

0148-0227/07/2005JD006981

Moore and Kleeman, 1996; *Samelson and Tziperman*, 2001; *McPhaden*, 2003, etc.], but debate remains concerning its cause. One of the possible causes is the rapid seasonal transition of monsoon circulation during the boreal spring that perturbs the Pacific basic state when the east-west sea surface temperature (SST) gradient is the weakest [*Webster and Yang*, 1992; *Lau and Yang*, 1996]. Another notion proposed by *Webster* [1995] is that SPB is due to the weakest ocean-atmosphere coupling during spring in the eastern Pacific. Other studies argued that SST anomalies in boreal spring are relatively small, such that these anomalies are difficult to be detected and forecasted in the presence of atmospheric and oceanic noises [*Xue et al.*, 1997; *Chen et al.*, 1995]. *Samelson and Tziperman* [2001] demonstrated that SPB is an inherent characteristic of ENSO, whereas *Chen et al.* [1995, 2004] suggested that this predictability barrier could be reduced through improving initialization. *McPhaden* [2003] showed that subsurface information has a winter persistence barrier and that the predictability of ENSO bestriding spring can be greatly enhanced by incorporating this information into the model. In general, the cause of the SPB remains elusive. There is an urgent need to further address the problems related to SPB for ENSO.

[5] Understanding of SPB can be gained by studying the initial error growth. *Moore and Kleeman* [1996] and *Samelson and Tziperman* [2001] have investigated the seasonal variability of ENSO error growth and explored the cause of predictability barrier by using linear singular vector (LSV). *Blumenthal* [1991], *Xue et al.* [1997], *Thompson* [1998], and *Moore and Kleeman* [1999] also used LSV to study ENSO predictability. LSV is one of the useful tools in predictability studies, but it deals with sufficiently small initial perturbations and thus is unable to describe nonlinear evolution of finite-amplitude initial perturbations [*Oortwijin and Barkmeijer*, 1995; *Mu et al.*, 2003].

[6] In this paper, we use conditional nonlinear optimal perturbation (CNOP) proposed by *Mu et al.* [2003] (see also *Mu and Zhang*, 2006) to study seasonal reliance of the evolution of finite-amplitude initial errors. The CNOP represents the initial error that has the biggest effect on the forecast results at the prediction time. CNOP method has been applied to study the ENSO precursor [*Duan et al.*, 2004] and the sensitivity of ocean thermohaline circulation to finite-amplitude perturbations [*Mu et al.*, 2004], as well as the passive variability of the thermohaline circulation [*Sun et al.*, 2005]. The aforementioned studies illustrate that CNOP is one of the useful tools for predictability study. A particular appealing aspect is that CNOP describes the optimal initial perturbation of nonlinear model and reveals the effect of nonlinearity on predictability.

[7] To facilitate theoretical understanding of essential dynamics and physics for ENSO predictability, we may apply CNOP method to a nonlinear ENSO model. The theoretical one developed by *Wang and Fang* [1996] may provide a convenient tool for analyzing the essential physics of SPB. *Burgers et al.* [2005] revealed SPB phenomenon by using the simplest ENSO recharge oscillator model advanced by *Jin* [1997a, 1997b], which is linear and consists of two-variable ordinary differential equations with stochastic forcing. The model of *Wang and Fang* [1996] (hereinafter referred to as WF96) is a nonlinear ENSO model of two-variable differential equations with self-sustained oscillation that may also capture the essential physical of SPB. In this research, we will use WF96 model to investigate SPB with CNOP approach.

[8] We briefly review the ideas of CNOP in the next section and introduce the ENSO model in section 3. Seasonality of the initial error growth for ENSO is examined in section 4. In section 5, we discuss the mechanism of the seasonal variation for error growth and explain the role of nonlinearity in error growth. We summarize the conclusions in section 6 and finally discuss the implication of our results in section 7.

2. Conditional Nonlinear Optimal Perturbation

[9] Let M_τ be the propagator of a nonlinear model from time 0 to τ. u_0 is an initial perturbation superimposed on the basic state $U(t)$, which is a solution to the nonlinear model and satisfies $U(t) = M_\tau(U_0)$, with U_0 being the initial value of basic state $U(t)$.

[10] For a chosen norm $\|\cdot\|$, an initial perturbation $u_{0\delta}$ is called CNOP if and only if

$$J(u_{0\delta}) = \max_{\|u_0\| \le \delta} \|M_\tau(U_0 + u_0) - M_\tau(U_0)\|, \tag{1}$$

where $\|u_0\| \le \delta$ is a constraint condition of initial perturbations defined by norm.

[11] CNOP is the initial perturbation whose nonlinear evolution attains the maximal value of the objective function J at time τ [*Mu et al.*, 2003; *Mu and Zhang*, 2006]. Nevertheless, there exists a possibility that J attains its local maximum in a small neighborhood of a point in the phase space. Such initial perturbation is called local CNOP. CNOP and local CNOP possess clear physical meanings. For example, in an anomaly model for ENSO, CNOP (local CNOP) superimposed on the climatological background state is most likely to evolve into El Niño (La Niña) event and acts as the optimal precursors of El Niño (La Niña) events [*Duan et al.*, 2004]. In this situation, CNOP can be considered to be the most predictable, meaning that if this signal related to CNOP is observed in nature, then the future outcome of the system is fairly certain. For the CNOPs superimposed on ENSO events, they describe initial errors that have largest effect on the prediction results of ENSO.

[12] In this paper, CNOP and local CNOP are computed by using sequential quadratic programming (SQP) solver [*Powell*, 1982], which is used to solve the nonlinear minimization problems with equality and/or inequality constraint condition. A brief description of the algorithm is referred to the study of *Mu et al.* [2003].

3. The Theoretical ENSO Model

[13] With adequate simplifications supported by observation, *Wang and Fang* [1996] distilled *Zebiak and Cane*'s [1987] intermediate coupled ocean-atmosphere model to a highly simplified one. The model consists of two dimensionless ordinary differential equations that describe, respectively, the temporal variations of the anomalous SST T

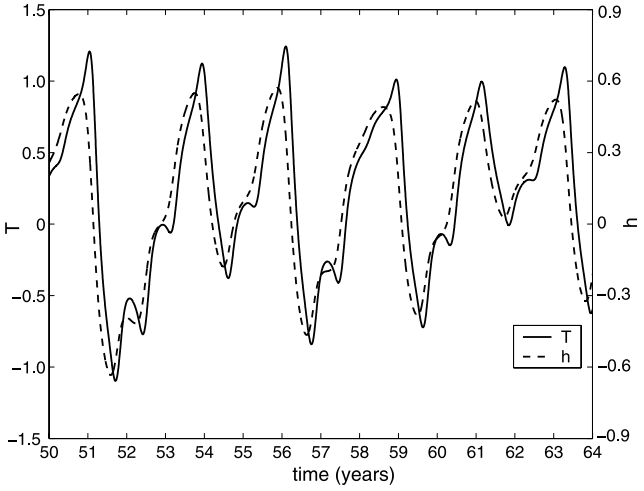

Figure 1. Time series of anomalous SST (solid line) and thermocline depth (dashed line) from model integration year 50 to year 64.

and thermocline depth h averaged in the equatorial eastern Pacific:

$$\begin{cases} \dfrac{\mathrm{d}T}{\mathrm{d}t} = a_1 T - a_2 h + \sqrt{\dfrac{2}{3}} T(T - a_3 h), \\ \dfrac{\mathrm{d}h}{\mathrm{d}t} = b(2h - T), \end{cases} \tag{2}$$

where $\mathrm{a}_1 = \overline{T}_z + \overline{T}_x - \alpha_\mathrm{s}$, $\mathrm{a}_2 = \mu\,\overline{T}_x$, $a_3 = \mu$, $b = \frac{2\alpha}{p(1-3\alpha^2)}$, and $p = (1-H_1/H)(L_0/L_s)^2$. For simplicity, the horizontal advection of temperature is neglected because it is relatively small compared to the vertical temperature advection and its effect can be incorporated into the nonlinear terms by modifying the coefficient μ [*Wang et al.*, 1999]. The linear coefficients a_1 and a_2 are determined by the basic state parameters $\overline{T}_x$ and $\overline{T}_z$, which characterize, respectively, the zonal temperature difference between the equatorial eastern and western basins and the vertical temperature difference between the basic state mixed-layer or SST and subsurface-layer water temperature. Note that these basic state parameters are time dependent, reflecting the climatological annual cycle of the basic state. α_s denotes Newtonian damping coefficient. α and μ are nondimensional coupling parameters. The parameter α represents an empirical air-sea coupling coefficient, and μ measures the degree of coupling between thermocline fluctuation and SST. The meanings of these parameters were listed in Table 1 of WF96; their typical values were derived empirically from observations or an intermediate tropical Pacific Ocean model [*Wang et al.*, 1995] driven by observed climatological monthly mean solar radiation, surface wind stress, and cloudiness forcing.

[14] The linear terms in the T equation describe the vertical advection by the anomalous upwelling of the mean SST ($\overline{T}_z$T) and the vertical advection by the mean upwelling of the anomalous SST ($\overline{T}_x(T - \mu h)$), and the Newtonian damping ($-\alpha_s T$). The quadratic term in T equation comes from the nonlinear temperature advection by anomalous upwelling of the anomalous temperature. The linear terms in h equation depict, respectively, the effect of equatorial waves on thermocline adjustment ($2bh$) and the effect of the zonal wind stress forcing via Sverdrup balance ($-bT$). The nondimensional parameter b is a nonlinear function of the air-sea coupling coefficient α and depends on scaling factors H (150 m, mean thermocline depth), H_1 (50 m mean mixed year depth), L_0 (300 km, the oceanic Rossby radius of deformation), and L_s (338 km, the meridional Ekman spreading length).

[15] WF96 used this dynamic system model to explain the cyclic, chaotic, seasonal-dependent evolution of ENSO. In the presence of the annual cycle, WF96 demonstrated that the solution of the dynamical system represents a strange attractor around a stable limit cycle in the phase plane; the corresponding solution in physical space represents an interannual oscillation with inherent deterministic chaos in amplitude and frequency. Furthermore, it was shown that the model ENSO cycle is phase-locked to the basic state annual cycle. To study the essential physics of ENSO predictability, *Mu and Duan* [2003] and *Duan et al.* [2004] utilized it to investigate the error growth for ENSO and to identify the precursors for ENSO events.

[16] Obviously, WF96 model is a highly simplified version of *Zebiak and Cane* [1987], in which ENSO oscillation may be much more regular than that in observations (Figure 1). Nevertheless, the interest of this study is the seasonality of ENSO predictability and its essential physics. Furthermore, the main characteristics related to seasonality shown by previous studies [*Webster and Yang*, 1992; *Moore and Kleeman*, 1996] may be roughly captured in WF96 model (see WF96 and section 4 in this paper). It is therefore suggested that this theoretical model is acceptable for exploring the fundamental physics of seasonality of error growth for ENSO qualitatively.

[17] The steady solution $O(0,0)$ of WF96 model means that the values of SSTA and thermocline depth anomaly are zero, which represents the climatological mean equilibrium state including annual cycle (see Figure 1 of WF96). The model is integrated numerically by using a fourth-order Runge-Kutta scheme with $\mathrm{d}t = 0.01$, which represents 1 day.

4. Dynamics of Season-Dependent Error Evolution for ENSO Events

[18] To understand SPB, it is necessary to investigate the seasonal dependence of error growth for ENSO events. Considering that CNOP is the initial error that has biggest the effect on prediction results, we compute CNOPs of ENSO events in WF96 model.

4.1. The Calculation of CNOPS of the ENSO Events

[19] Let u_0 be an initial error of a predetermined ENSO event. We adopt equation (1) as the objective function to compute its CNOP. In this situation, U_0 in equation (1) represents the initial state of the model ENSO, and J determines the maximum prediction error of ENSO event. The error evolution is measured by using norm $\|u(t)\| = \sqrt{(T')^2 + (h')^2}$, where T' and h' are the errors of SSTA and thermocline depth anomaly, respectively.

[20] With the above chosen norm, *Duan et al.* [2004] have investigated the CNOPs superimposed on annual cycle in WF96 model. The results demonstrated that for the annual cycle, regardless of what initial time is, there exist

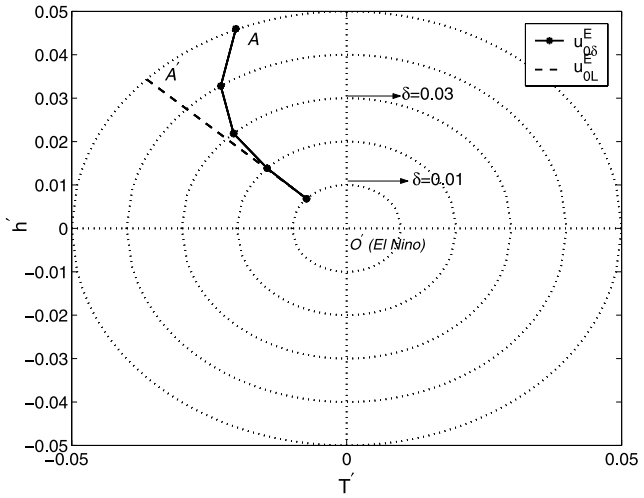

Figure 2. Phase distribution of CNOPs (solid line) and corresponding LSVs (dashed line) superimposed on El Niño event U_J^E. δ denotes the magnitude of CNOP and the corresponding LSV measured by the chosen norm. O' labeled by "El Niño" represents the above basic state El Niño event.

CNOPs and local CNOPs for the different optimization time intervals. These CNOPs (local CNOPs) have the robust patterns of negative (positive) SST and positive (negative) thermocline depth anomalies. They are most likely to evolve into El Niño (La Niña) events and therefore provide the optimal precursors of El Niño (La Niña) events within WF96 model, which agrees with the observations qualitatively.

[21] Considering the time period during which the ENSO optimal precursors arise qualitatively in observation [*Duan et al.*, 2004], we choose El Niño (La Niña) events with optimal precursors occurring in January (October) to study the error development aftermath. These El Niño (La Niña) events are denoted as U_J^E (U_J^L) and U_O^E (U_O^L), respectively. El Niño events U_J^E (U_O^E) tend to peak about a year later in December (October). In *T-h* phase space, the precursors of these El Niño events can be expressed as (−0.1373, 0.1968) and (−0.0283,0.2383), respectively, for magnitude of norm being 0.24; the ones of La Niña events are (0.1511, −0.1865) and (0.0776, −0.2271), respectively. Details can be seen in the work of *Duan et al.* [2004].

[22] Now we compute the CNOPs superimposed on the model El Niño (La Niña) events, U_J^E (U_J^L) and U_O^E (U_O^L), where the time interval length is a year and the constraint is $\|u_0\| \leq \delta$, with δ ranging from 0.01 to 0.05. The results show that for each basic state El Niño (La Niña) event, there exists a CNOP, denoted by $U_{0\delta}^E$ (U_J^L). These CNOP-type errors robustly perturb SSTA negatively and thermocline depth anomaly positively at initial time (Figures 2 and 3). For example, for El Niño event U_J^E, the CNOPs with $\delta = 0.01$, 0.02, 0.03, 0.04, and 0.05 are (−0.0072, 0.0065), (−0.0142, 0.0137), (−0.0206, 0.0218), (−0.0204, 0.03451), and (−0.0201, 0.0456), respectively, whereas the ones of La Niña U_J^L are (−0.0071, 0.0069), (−0.0145, 0.0137), (−0.0227, 0.0198), (−0.0311, 0.0252), and (−0.0396, 0.0308). Furthermore, these CNOP-type errors of El Niño and La Niña, after about 1–2 months, all evolve to perturb positively SSTA and thermocline depth anomaly within the given finite time periods (the figures are not shown).

[23] To compare CNOP of El Niño (La Niña) with LSV, we investigate the distribution of CNOP and LSV in phase space (T', h'). $u_{0L} = (-0.0107, 0.0102)$ is an LSV of El Niño U_J^E and is located in quadrant II, which is the fastest growing perturbation of the tangent linear model (TLM) of WF96 model with respect to U_J^E. We define the scaled LSVs,

$$u_{0L}^E = \frac{\|u_{0\delta}^E\|}{\|u_{0L}\|} u_{0L},$$

thus

$$\|u_{0L}^E\| = \|u_{0\delta}^E\| = \delta.$$

[24] This means that the CNOP and the scaled LSV of the El Niño are of the same magnitude of norm. Figure 2 illustrates them for the different values of δ, where A and A' correspond to the $U_{0\delta}^E$ and $U_{0L}{}^E$ with $\delta = 0.05$, respectively. It is readily shown that for the same value of δ, when δ is relatively large, for instance, $\delta = 0.04$ or 0.05 (i.e., the SSTA component of the initial error is confined to be smaller than dimensional 0.08° or 0.1°C), the CNOP $U_{0\delta}^E$ is quite different from the scaled LSV U_{0L}^E. With δ increasing from 0.01 to 0.05, the LSVs show themselves a beeline, while the CNOPs shape into a curve. Then the differences between CNOP and LSV become progressively large with increasing δ. This indicates that the larger the initial error, the more considerable the differences between CNOP and LSV. Similar analysis is performed to the La Niña event U_J^L. The results show that the CNOPs are different from the corresponding LSVs although these differences are relatively small compared to those of El Niño (Figure 3).

[25] We also examine the differences between CNOPs and LSVs for El Niño events U_O^E and La Niña events U_O^L,

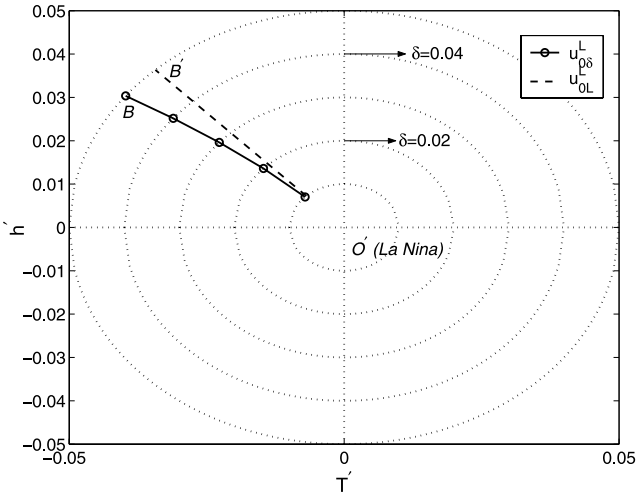

Figure 3. Phase distribution of CNOPs (solid line) and corresponding LSVs (dashed line) superimposed on La Niña event U_J^L. δ is same as that in Figure 1. O' represents the La Niña event.

Table 1. The Values of κ Corresponding to El Niño Event U_O^E

δ	OND	JFM	AMJ	JAS
0.01	1.4028	2.8391	6.5385	0.6932
0.03	1.3908	2.8636	8.2698	1.9113
0.05	1.3788	2.8863	10.1690	3.8327
LSV-L	1.4084	2.8264	6.2295	0.6898
LSV-N	1.4083	2.8618	8.8971	2.0312
P_E^1	1.0871	1.0988	5.9867	1.5473
P_E^2	1.3658	2.7866	4.7889	0.9804
P_E^3	1.1180	0.8400	2.4800	−0.2879
P_E^4	1.3567	1.0978	1.2087	0.0059

Table 2. The Values of κ Corresponding to La Niña Event U_O^L

δ	OND	JFM	AMJ	JAS
0.01	1.5847	2.3371	1.2026	0.8932
0.03	1.5738	2.3712	1.2977	0.9113
0.05	1.5628	2.4051	1.4104	0.9327
LSV-L	1.5982	2.3264	1.1954	0.8398
LSV-N	1.5813	2.3436	1.3920	0.8722
P_L^1	1.0800	0.4580	0.2180	0.1089
P_E^2	1.6520	1.7180	0.3440	0.4832
P_E^3	1.0802	0.4587	0.2089	0.1188

respectively. Similar results are obtained. The details are therefore not shown here.

4.2. Seasonal Dependence of Initial Error Growth of ENSO Events

[26] In the scenario of perfect model, the model ENSO events, which are obtained by integrating the model with proper initial conditions, could be considered as a "hindcast mode" to be predicted with uncertain initial fields. Along this thinking, *Duan and Mu* [2005] estimated the predictability of WF96 model by predicting the maximum predictable time of model ENSO event. Their results indicated that the ENSO warm event is hardly predictable through spring and exhibits the behavior of SPB.

[27] In this section, we will investigate the season-dependent predictability of model ENSO events by estimating the uncertainties caused by initial error. A calendar year is divided into four seasons starting with January to March (JFM), followed by April to June (AMJ), and so forth. Then we investigate the slopes of the curve $\gamma_\delta(t) = \frac{\|u_{N\delta}(t)\|}{\delta}$ at different seasons, where $u_{N\delta}(t)$ represents the nonlinear evolution of CNOP for ENSO. The slope of $\gamma_\delta(t)$ is denoted by κ and indicates the growth tendency of CNOP normalized by δ at different seasons. A positive (negative) value of κ corresponds to an increase (decrease) of the errors, and the larger the absolute value of κ, the faster the increase (decrease) of the errors.

[28] Tables 1 and 2 show the slopes of $\gamma_\delta(t)$ for El Niño event U_O^E and La Niña event U_O^L. Here, the values of κ related to LSV-L are the slopes of the curve $\gamma_L(t) = \frac{\|u_L(t)\|}{\|u_{0L}\|}$ at different seasons; u_{0L} and u_L (t) represent the LSV of El Niño (or La Niña) and its linear evolution. Note that for any constant c, initial error cu_{0L} is also an LSV due to the linearity; its linear evolution can be expressed as $c\|u_L(t)\|$. It is easily derived that the curve $\gamma_L(t)$ is independent of the constant c, whose slopes at each season are therefore invariant for the different LSVs.

[29] From Table 1, it is demonstrated that the largest growth of CNOP occurs during AMJ season (boreal spring) for the El Niño U_O^E. Although the largest error growth of El Niño during AMJ is also shown by LSV and TLM, the nonlinear growth of CNOP is different from the linear counterpart of LSV. Moreover, with the magnitude of initial errors increasing from 0.01 to 0.05, the differences between the results of CNOP and LSV become more and more considerable. The implication is that within this simple model, nonlinearity plays an important role in the predictability of El Niño U_O^E for the large initial errors. It enhances aggressively the error growth of El Niño and increases the uncertainties of El Niño forecast bestriding AMJ season. For La Niña event U_O^L, the results shown in Table 2 demonstrate that the seasonal dependence of error evolution is less prominent than that of El Niño. In addition, nonlinearity is trivially important in error growth of La Niña over the whole interval of δ.

[30] We also investigate the slopes κ of large ensemble of initial errors, including LSV in the domain $\|u_0\| \le \delta$ with different values of δ. The results suggest that not all initial errors can give rise to such prominent season-dependent evolution as those of the CNOPs of El Niño. To show the results, we list in Table 1 the slopes of some representatives of initial errors u_0, which are P_E^1: (0.0201, 0.0456), P_E^2: (0.0396, −0.0308), P_E^3: (−0.0396, −0.0308), and P_E^4: (−0.0021, −0.0499). As a sufficient comparison, we also give the results of season-dependent evolution of LSV in nonlinear model (see the "LSV-N" in Tables 1 and 2). These initial errors are of the norm magnitude of 0.05. Comparisons between the CNOP and the large ensemble of initial errors (including LSV) demonstrate that CNOP most likely induces the prominent seasonal variation of error evolution for El Niño. The remaining initial errors including LSV either have somewhat smaller slopes or have neutral ones during AMJ. In particular, the growth of initial error P_E^4 in AMJ is even less than that in October to December (OND) season.

[31] The seasonal variations of the CNOPs of the El Niño (La Niña) events U_J^E (U_J^L) are also investigated (Tables 3 and 4). The results are similar to those of U_O^E (U_O^L): the CNOP of El Niño exhibits a prominent season variation, while that of La Niña displays a less prominent one. However, in this case, nonlinearity plays a minor role in the error growths of El Niño during AMJ season. The LSV growth for El Niño during spring is trivially smaller than the CNOP growth for El Niño.

Table 3. The Values of κ Corresponding to El Niño Event U_J^E

δ	JFM	AMJ	JAS	OND
0.01	1.2051	4.1555	2.2042	0.0981
0.03	1.2059	4.1736	2.3686	0.3781
0.05	1.2068	4.1875	2.5377	0.8190
LSV-L	1.2047	4.1450	1.9793	0.0842
LSV-N	1.2044	4.1477	2.5223	0.6318
P_E^1	1.2028	4.1211	2.1316	0.0361
P_E^2	1.3969	2.8839	2.0363	−0.3212
P_E^3	1.4049	2.9854	1.1142	−0.9764
P_E^4	1.5035	1.4871	1.1036	0.0056

Table 4. The Values of κ Corresponding to La Niña Event U_J^L

δ	JFM	AMJ	JAS	OND
0.01	1.6569	2.7077	0.1402	1.1249
0.03	1.6604	2.7139	0.1429	1.1669
0.05	1.6638	2.7251	0.1642	1.2086
LSV-L	1.6532	2.7040	0.1412	1.1047
LSV-N	1.6568	2.7189	0.1517	1.1347
P_E^1	1.6638	2.7104	0.1028	1.3026
P_E^2	1.6461	2.6693	−0.2542	−0.0003
P_E^3	1.6258	2.6133	−0.2346	−1.0036

[32] Quite a few authors, i.e., *Moore and Kleeman* [1996], *Chen et al.* [1997], etc., studied the role of climatological mean state in the error growth of ENSO predictions. The CNOP-type errors are novel ones, and the effect of climatological background state on their evolutions is investigated by two kinds of experiments. First, we shift the phase of annual cycle forward by 6 months. Then the northern fall becomes the most unstable season, and the warming tends to start in November. In this case, we find out that the largest error growth of El Niño appears in the OND season and phase-locks to the annual cycle. Second, we study the case of climatological background state being an annual mean state instead of an annual cycle. It is shown that the CNOP growth for El Niño has no obvious seasonal dependence. For simplicity, we only report the results of these experiments and do not show the details.

[33] The above results demonstrate that CNOPs of two types of El Niño events show prominent season-dependent evolutions with maximum error growth occurring during AMJ season on the onset phase of them. Different initial uncertainties of ENSO may induce varying degrees of seasonal variation of the error evolution. CNOP of El Niño has the potential to induce the pronounced seasonal variability. Especially, in the season-dependent error evolution of El Niño U_O^E, the spring growth of CNOP is significantly larger than those of LSVs for the finite amplitude of initial errors. The other initial errors have either less prominent season-dependent evolution or neutral ones. However, for the La Niña events, even if the initial error is taken to be the type of CNOPs, the error evolution displays a less prominent seasonal dependence. The above analysis distinguishes not only the differences of the season-dependent error evolutions of El Niño and La Niña events but also the distinct characteristics of season-dependent evolutions of different-type initial errors of El Niño. Furthermore, it also identifies the role of climatological annual cycle in SPB. To sum up, the largest error growth of ENSO results from the combined effect of these three factors. The nonlinearity within WF96 model enhances largely the error growth of some El Niño events and increases the uncertainty of ENSO prediction bestriding spring. CNOP stands for the initial error that induces the most prominent seasonality of error growth for El Niño.

5. The Mechanism Responsible for Error Growth and SPB of ENSO Events

[34] In this section, we will explain why the largest error growth of El Niño occurs during the AMJ season and how the nonlinearity increases the uncertainties of ENSO forecast bestriding AMJ.

5.1. The Mechanism Causing the Largest Error Growth of ENSO Warm Event During AMJ Season

[35] Let (T, h) and $(T + T', h + h')$ be the solutions of the WF96 model. By subtracting $\frac{dT}{dt}$ and $\frac{dh}{dt}$ from $\frac{d(T+T')}{dt}$ and $\frac{d(h+h')}{dt}$, respectively, we obtain the governing equations of (T', h')

$$\begin{cases} \dfrac{dT'}{dt} = A_1 T' - A_2 h' + \sqrt{\dfrac{2}{3}} T'(T' - a_3 h') \\ \dfrac{dh'}{dt} = b(2h' - T'), \end{cases} \tag{3}$$

where $A_1 = a_1 + \sqrt{\frac{2}{3}}\,(2T - a_3 h)$, $A_2 = a_2 + \sqrt{\frac{2}{3}}\,a_3 T$, and a_3 and b are the same as those in equation (2). If (T, h) are assumed to be a "true state" (basic state) to be predicted, (T', h') can be understood as the uncertainty superimposed on "true state". Then equation (3) describes the evolution of the uncertainty. To study the predictability of El Niño or La Niña, we suppose that the "true state" is the above El Niño or La Niña events. One of the steady solutions in equation (3) is the origin in phase space and represents El Niño or La Niña events in which the errors of both SSTA and h are zero.

[36] From equation (3), we derive the tendency equations of error evolution (the details are in Appendix)

$$S = \frac{1}{2}\frac{d(T'^2 + h'^2)}{dt} = C + E + P$$

where

$$C = a_1 T'^2 - a_2 T' h' + b h'(2h' - T'), \tag{4}$$

$$E = \sqrt{\frac{2}{3}}(2T - a_3 h)T'^2 - \left(\sqrt{\frac{2}{3}} a_3 T\right) T' h', \tag{5}$$

$$P = \sqrt{\frac{2}{3}} T'^2 (T' - a_3 h'). \tag{6}$$

The values of S are reflected proportionally by the slopes κ in Tables 1, 2, 3, and 4. In fact, the slopes κ are equivalent to the mean values of S/δ in each season (δ is referred to section 4), from which we know that the time-dependent S exhibits prominent seasonal variation when El Niño and its CNOPs are applied to S.S can be divided into three parts: C, E, and P. The term C includes the model coefficients a_1 and a_2, which are linked with the climatological mean state in WF96 model. It is conceivable that C denotes the effects of climatological mean state on the error evolution of ENSO. Similarly, since the expression E is embedded with T and h, it can be understood as the effect of ENSO event on its uncertainties. The term P is also associated with the error of ENSO and reflects the role of the nonlinearity in error evolution. Note that the magnitudes of C, E, and P depend on the initial error pattern. Thus S shows that the error

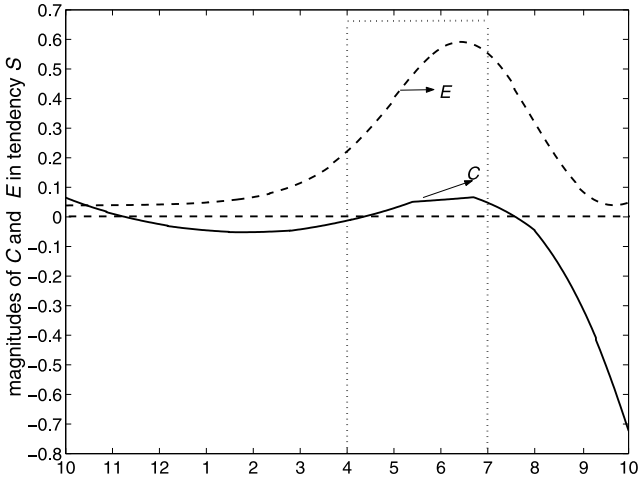

Figure 4. Magnitudes of C and E related to CNOP of El Niño U_O^E, where the magnitude of CNOP measured by norm is 0.05. The rectangle marks the period of boreal spring.

growth of ENSO not only depends on the climatological mean state but also depends on the ENSO events themselves and their initial error pattern. Furthermore, nonlinearity is also an important factor in controlling error evolution. Then with what manner the CNOP growth depends on these factors?

[37] The numerical results in section 4.2 demonstrate that the nonlinearity enhances the CNOP growth of El Niño during AMJ at the onset of El Niño. This indicates that the nonlinear term $\eta(T', h') = T'(T' - a_3 h')$ in equation (3) is positive during AMJ (the theoretical analysis can be seen in section 5.2). Section 4.1 shows that both T' and h' components of CNOP-type error develop to be positive after 1–2 months, so $T'(t)$ and $h'(t)$ during AMJ are both positive for model El Niño, U_J^E and U_O^E. Then the inequality $T' > a_3 h'$ holds. Furthermore, *Duan et al.* [2004] demonstrated that during the same period, the El Niño was also enhanced by the nonlinearity. The nonlinear term in WF96 model $T(T - a_3 h) > 0$ and then the inequality $T > a_3 h$ holds with $T(t) > 0$ and $h(t) > 0$ during AMJ. By these conditions, it is proved that all of C, E, and P are positive during AMJ for the above El Niño events and their CNOPs (see the Appendix). Furthermore, the largest values of C and E arise in AMJ season (Figure 4). This implies that the conditions of both climatological mean state and El Niño event during AMJ are most favorable for the CNOP growth.

[38] For the term $P > 0$, it indicates that the nonlinear temperature advection for El Niño amplifies the evolution of the CNOP-type error during spring. It should be pointed out that the figure of P related to CNOP resembles that of the nonlinear term in equation (3) (shown in Figure 7) except for its magnitude (the figure is therefore omitted). Therefore, we obtain that although P is positive during spring and enhances the error growth, its magnitude is not the largest during spring and does not play the dominant role in seasonality of ENSO predictability. Nevertheless, the effect of nonlinearity on error growth cannot be neglected since it amplifies the error growth of El Niño during AMJ, which will be discussed in detail in section 5.2.

[39] Therefore, it is derived that the spring strongest ocean-atmospheric coupled instability of climatological mean state and the weakest persistence of El Niño play the most important role in seasonal variation of CNOP growth.

[40] To investigate the dependence of SPB on the initial error patterns, we plot E and C of the tendency S in Figure 5 for the initial error P_4 (−0.0021, −0.0499) of El Niño U_O^E in section 4. It shows that E and C become quite small compared with those of CNOP. In this case, the combined effect of climatological mean state and El Niño event cannot make S of P_4 to be the largest during AMJ. Besides, we have also found out that the magnitude of P related to P_4 is relatively small during spring compared with that of CNOP. These suggest that the largest error growth of El Niño is also closely related to the type of the initial error.

5.2. The Role of the Nonlinearity in Error Growth of El Niño

[41] It follows from the above sections that CNOP growth of El Niño U_O^E during AMJ season is substantially larger than the corresponding LSV growth for large-amplitude initial uncertainties. This suggests that the nonlinearity plays an important role in error growth of some El Niño events. As for the La Niña events, the growth of CNOP during AMJ is only moderately larger than that of LSV, and the effect of nonlinearity on error growth of La Niña is negligible. To make these much clear, we analyze theoretically the role of nonlinearity in ENSO predictability.

[42] Equation (3) has two characteristic lines given by $\frac{dT'}{dt} = 0$ and $\frac{dh'}{dt} = 0$, i.e.,

$$h' = \frac{\left(A_1 - \sqrt{\frac{2}{3}}T'\right)T'}{A_2 + a_3\sqrt{\frac{2}{3}}T'} = f(T'),\ or,\ T' = f^{-1}(h')$$

$$h' = \frac{1}{2}T'.$$

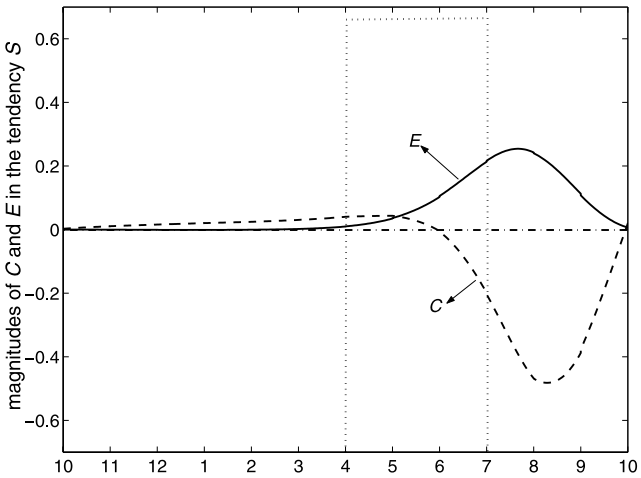

Figure 5. Magnitudes of C and E related to initial error P_4 (−0.0021, −0.0499) of El Niño U_O^E, where the magnitude of P_4 is the same as that of CNOP in Figure 4. The rectangle marks the period of boreal spring.

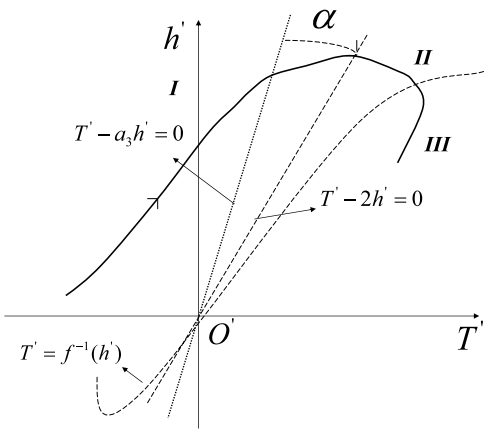

Figure 6. Schematic diagram showing the phase of CNOP evolution for ENSO warm event.

These two lines partition the phase plot of $T'(t)$ and $h'(t)$ into three parts (see Figure 6). Besides, we note that T' equation in equation (3) characterizes the nonlinearity. In addition, it can be rewritten as follows:

$$\frac{dT'}{dt} = A_1 T' - A_2 h' + \eta(T', h'), \tag{7}$$

where $\eta(T',h') = \sqrt{\frac{2}{3}}\, T'\,(T' - a_3 h')$ and represents the nonlinear temperature advection. On the line $T' = a_3 h'$, equation (7) becomes a linear one. To facilitate the discussion, we plot this line in Figure 6 too.

[43] It is shown from Figure 6 that when the CNOP-type error for El Niño develops to the period of α, its SSTA component $T'(t) > 0$ and satisfies $a_3 h' < T' < 2h'$. This makes $\eta(T', h') > 0$. From equation (7), it is derived that the larger the nonlinear term $\eta(T', h')$, the larger the error growth of SSTA. Besides, during the period of α, the variations of T' and h' tend to be a positive feedback. Therefore, when T' becomes large, h' and then the error $E(t) = \sqrt{(T')^2 + (h')^2}$ also increase. Consequently, the larger the nonlinear term, the larger the error growth for El Niño. If the nonlinear effect is ignored in equation (7), the error growth will be smaller than that with positive nonlinear term. Thus we have explained why the nonlinearity enhances the error growth of El Niño event. Figure 7 demonstrates that the larger the CNOP-type errors, the larger the nonlinear term, and then the stronger the effects of the nonlinearity on the spring error growth of El Niño.

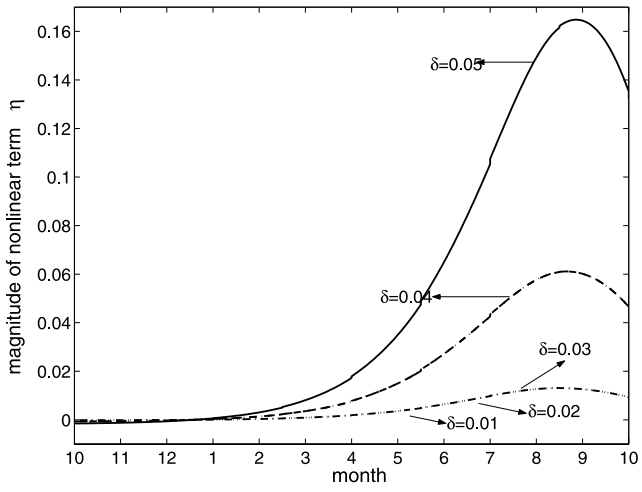

Figure 7. Magnitudes of nonlinear term in equation (3) with El Niño U_O^E, which is obtained by integrating equation (3) with the CNOPs of U_O^E being initial values. δ indicates the magnitudes of CNOP in terms of the chosen norm.

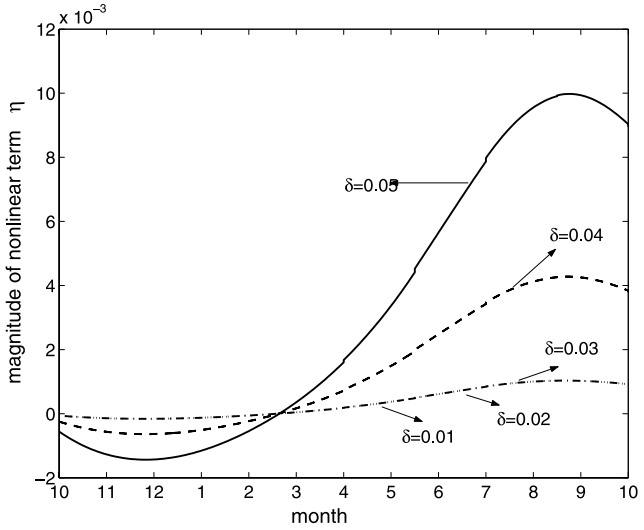

Figure 8. Magnitudes of nonlinear term in equation (3) with La Niña U_O^L, which is gained by integrating equation (3) with the CNOPs of U_O^L being initial values. δ is the same as in Figure 7.

[44] As for the CNOP-type error of La Niña, for the different amplitudes of initial uncertainties, although the nonlinear term is also larger than zero during AMJ, it is always quite small and even negligible (Figure 8). In this case, nonlinearity plays a minor role. This interprets why the CNOP growth of La Niña during spring does not differ significantly from the corresponding LSV growth.

[45] The importance of nonlinearity in error growth for El Niño can also be observed from the relationship of three parts in tendency S. We have tested that all of C, E, and P are positive during spring and have the relationship of $E > P > C$ for CNOP of El Niño. Obviously, P is not small. This implies that the effect of nonlinearity on El Niño predictability is important although it does not play the dominant role in SPB.

6. Conclusion

[46] Seasonal variability of ENSO predictability and the related spring predictability barrier (SPB) problem were studied by analyzing the properties of initial error growth of El Niño and La Niña events in a theoretical ENSO model. The results show that the largest growth rate of the conditional nonlinear optimal perturbation (CNOP) for El Niño occurs during April-May-June, which coincides with the time of the predictability barrier of many ENSO predictions. With increasing magnitude of CNOPs, the amplitude of spring error growth for El Niño becomes progressively large. Although the largest error growth of El Niño during

AMJ is also shown through linear singular vector (LSV), the CNOP growth is significantly larger than that of the LSV for large-amplitude initial perturbations in model El Niño events. This implies that the nonlinearity plays an important role in error evolution of ENSO warm event. Nonlinearity related to temperature advection enhances spring error growth of El Niño and increases the forecast uncertainties of ENSO bestriding spring.

[47] Furthermore, we compared the seasonal variations of the CNOP growth for ENSO with those of a large ensemble of initial errors chosen randomly from a constrained initial domain. It is demonstrated that not all initial errors tend to induce prominent season-dependent evolution; it is the CNOP superimposed on an El Niño condition that yields such phenomenon. However, for the La Niña events, even if the initial errors are taken to be of the types of CNOPs, their evolutions do not exhibit notable seasonal dependence.

[48] The role of climatological annual cycle in SPB was also examined, which demonstrates that the largest error growth in El Niño is robustly phase-locked to the phase of annual cycle.

[49] In summary, the SPB may result from the combined effect of three factors: the climatological annual cycle, the El Niño event itself, and the initial error pattern. CNOP-type error represents the initial error pattern that most likely induces the SPB for El Niño. There exist other kinds of initial error patterns that do not show apparent seasonal variation in error growth. We conceive that if the initial error is not of the CNOP-type, the ENSO prediction could be less uncertain. It is therefore suggested that if a data assimilation method could filter CNOP-type initial errors, then ENSO predictability could be improved.

7. Discussion

[50] A large body of previous studies investigated SPB for ENSO. *Moore and Kleeman* [1996], *Chen et al.* [1997], and *van Oldenborgh et al.* [1999] demonstrated the roles of both the phase of the climatological basic state and that of the El Niño in SPB. Then *Goswami et al.* [1997], *van Oldenborgh et al.* [1999], and *Fan et al.* [2000] pointed out the importance of the initial fields in SPB [see also *Tang et al.*, 2003]. Our results suggest that the combined effects of the above three factors give rise to the SPB.

[51] Recently, *Galanti et al.* [2002] and *Burgers et al.* [2005] investigated the linear error growth of ENSO caused by two different kinds of linear coupled instability. Our results demonstrate that nonlinearity can amplify the linear error growth for some El Niño events and increases the uncertainties of ENSO forecast bestriding boreal spring. We also find out that CNOP is superior to LSV in describing the initial error growth that induces prominent SPB for El Niño. Other types of initial errors have either relatively weak season-dependent evolution or neutral ones.

[52] It is of importance to realize that the results were derived from a simple theoretical model, which is a highly simplified version of *Zebiak and Cane* [1987], and the complex aspects of ENSO cannot be fully described. Only two variables were retained in the equations, of which the dynamics was simplified considerably. Consequently, CNOPs of WF96 model cannot give a spatial picture of initial error, while *Xue et al.* [1997] and *Blumenthal* [1991] presented the initial error spatial structure by solving LSV of the model of *Zebiak and Cane* [1987]. The nonlinear term is also a highly parameterized form of nonlinear advection in the eastern Pacific. Furthermore, WF96 model only describes the variation of equatorial eastern Pacific and cannot identify the roles of the uncertainties in the central and western Pacific in ENSO predictability. Nevertheless, considering other additional studies that emphasized the important effects of the uncertainties in the eastern Pacific (see the discussion in the study of *Samelson and Tziperman* [2001]), the results obtained by using WF96 model is also instrumental for understanding ENSO predictability.

[53] Considering the limit of the adopted model, it would be desirable to use more complex coupled ones to carry out further studies. The role of atmospheric variability related to westerly wind events or MJO in limiting ENSO predictability is another area of interest. The uncertainties caused by stochastic forcing can be understood as a kind of model error. The influence of stochastic forcing on ENSO predictability is still elusive [*Flügel et al.*, 2004; *Zavala-Garay et al.*, 2004], which deserves future studies.

Appendix A: Properties of the Terms in Tendency Equation S

[54] By multiplying T' and h' equations in equation (3) with T' and h', respectively, it becomes

$$\begin{cases} T'\dfrac{\mathrm{d}T'}{\mathrm{d}t} = T'(A_1T' - A_2h' + \sqrt{\dfrac{2}{3}}T'(T' - a_3h')), \\ h'\dfrac{\mathrm{d}h'}{\mathrm{d}t} = bh'(2h' - T'). \end{cases}$$

Then we derive $S = \frac{1}{2}\frac{\mathrm{d}(T'^2+h'^2)}{dt} = C + E + P$, which are defined in equations (3)–(5).

A1. The Proof of $E > 0$ During AMJ

[55] By applying spring conditions $T > 0$, $T' > 0$, $T > a_3h$, and $T' > a_3h'$ in section 5.1 to

$$\begin{aligned} E &= \sqrt{\tfrac{2}{3}}(2T - a_3h)T'^2 - \left(\sqrt{\tfrac{2}{3}}a_3T\right)T'h' \\ &= \sqrt{\tfrac{2}{3}}(2T - a_3h)T'\left[T' - \tfrac{a_3T}{2T - a_3h}h'\right], \end{aligned}$$

we can obtain that

$$E > \sqrt{\frac{2}{3}}(2T - T)T'\left(T' - \frac{a_3T}{2T - T}h'\right) = \sqrt{\frac{2}{3}}TT'(T' - a_3h') > 0.$$

A2. The Proof of $P > 0$ During AMJ

[56] From the condition $T' > a_3h'$, it is easily derived that $P = \sqrt{\frac{2}{3}}\,T'^2\,(T' - a_3h') > 0$.

A3. The Proof of $C > 0$ During AMJ

[57] According to the typical values of the parameters listed in Table 1 of WF96, we know that $a_1 \approx 0$ and $a_2 < 0$ during AMJ. Furthermore, the evolutions of T' and h' for El

Niño tend to be a positive feedback during AMJ. It implies that when $\frac{dT'}{dt} > 0$ and $\frac{dh'}{dt} > 0$, then $2h' > T'$ holds [see h' equation in equation (3)]. Upon these facts and the spring conditions $T' > 0$ and $h' > 0$, we obtain that

$$C = a_1 T'^2 - a_2 T' h' + b h' (2h' - T') > 0.$$

[58] **Acknowledgments.** The authors are grateful to the three anonymous reviewers for their useful suggestions. This work was jointly supported by KZCX3-SW-230 of Chinese Academy of Sciences and the National Nature Scientific Foundation of China (40233029, 40505013, and 40221503). Bin Wang acknowledges the support from the NOAA Pacific program.

References

Battisti, D. S., and A. C. Hirst (1989), Interannual variability in a tropical atmosphere-ocean model: Influence of the basic state, ocean geometry and nonlinearity, *J. Atmos. Sci.*, *46*, 1687–1712.

Blumenthal, M. B. (1991), Predictability of a coupled ocean-atmosphere model, *J. Climate*, *4*, 766–784.

Burgers, G., F. F. Jin, and G. J. van Oldenborgh (2005), The simplest ENSO recharge oscillator, *Geophys. Res. Lett.*, *32*, L13706, doi:10.1029/2005GL022951.

Cane, M. A., S. E. Zebiak, and S.C. Dolan (1986), Experimental forecasts of El Nino, *Nature*, *321*, 827–832.

Chen, D., S. E. Zebiak, A. J. Busalacchi, and M. A. Cane (1995), An improved procedure for El Nino forecasting, *Science*, *269*, 1699–1702.

Chen, Y., D. S. Battisti, T. N. Palmer, J. Barsugli, and E. S. Sarachik (1997), A study of the predictability of tropical Pacific SST in a coupled atmosphere-ocean model using singular vector analysis: The role of the annual cycle and the ENSO cycle, *Mon. Weather Rev.*, *125*, 831–845.

Chen, D., M. A. Cane, A. Kaplan, S. E. Zebiak, and D. J. Huang (2004), Predictability of El Nino over the past 148 years, *Nature*, *428*, 733–736.

Duan, W. S., and M. Mu (2005), Investigating decadal variability of El Nino-Southern Oscillation asymmetry by conditional nonlinear optimal perturbation, *J. Geophys. Res.*, *111*, C07015, doi:10.1029/2005JC003458.

Duan, W. S., M. Mu, and B. Wang (2004), Conditional nonlinear optimal perturbation as the optimal precursors for ENSO events, *J. Geophys. Res.*, *109*, D23105, doi:10.1029/2004JD004756.

Fan, Y., M. R. Allen, D. L. T. Anderson, and M. A. Balmaseda (2000), How predictability depends on the nature of uncertainty in initial conditions in a coupled model of ENSO, *J. Climate*, *13*, 3298–3313.

Flügel, M., P. Chang, and C. Penland (2004), The role of stochastic forcing in modulating ENSO predictability, *J. Climate*, *17*, 3125–3140.

Galanti, E., E. Tziperman, M. Harrison, A. Rosati, and R. Giering (2002), The equatorial thermocline outcropping—A seasonal control on the tropical Pacific Ocean-atmosphere instability strength, *J. Climate*, *15*, 2721–2739.

Goswami, B. N., K. Rajendran, and D. Sengupta (1997), Source of seasonality and scale dependence of predictability in a coupled ocean-atmosphere model, *Mon. Weather Rev.*, *125*, 846–858.

Jin, F. F. (1997a), An equatorial ocean recharge paradigm for ENSO. Part I: Conceptual model, *J. Atmos. Sci.*, *54*, 811–829.

Jin, F. F. (1997b), An equatorial ocean recharge paradigm for ENSO. Part II: A stripped-down coupled model, *J. Atmos. Sci.*, *54*, 830–847.

Kirtman, B. P., J. Shukla, M. Balmaseda, N. Graham, C. Penland, Y. Xue, and S. Zebiak (2002), Current status of ENSO forecast skill: A report to the Climate Variability and Predictability (CLIVAR) Numerical Experimentation Group (NEG), CLIVAR Working Group on Seasonal to Interannual Prediction, Clim. Variability and Predictability, Southampton Oceanogr. Cent., Southampton, UK.

Kleeman, R., A. M. Moore, and N. R. Smith (1995), Assimilation of sub-surface thermal data into an intermediate tropical coupled ocean-atmosphere model, *Mon. Weather Rev.*, *123*, 3103–3113.

Lau, K.-M., and S. Yang (1996), The Asian monsoon and predictability of the tropical ocean-atmosphere system, *Q. J. R. Meteorol. Soc.*, *122*, 945–957.

McCreary, J. P., and D. L. T. Anderson (1991), An overview of coupled ocean: C atmosphere models of El Nino and the Southern Oscillation, *J. Geophys. Res.*, *96*, 3125–3150.

McPhaden, M. J. (2003), Tropical Pacific Ocean heat content variations and ENSO persistence barriers, *Geophys. Res. Lett.*, *30*(9), 1480, doi:10.1029/2003GL016872.

Moore, A. M., and R. Kleeman (1996), The dynamics of error growth and predictability in a coupled model of ENSO, *Q. J. R. Meteorol. Soc.*, *122*, 1405–1446.

Moore, A. M., and R. Kleeman (1999), The nonnormal nature of El Nino and intraseasonal variability, *J. Climate*, *12*, 2965–2982.

Mu, M., and W. S. Duan (2003), A new approach to studying ENSO predictability: Conditional nonlinear optimal perturbation, *Chin. Sci. Bull.*, *48*, 1045–1047.

Mu, M., and Z. Y. Zhang (2006), Conditional nonlinear optimal perturbation of a barptrophic model, *J. Atmos. Sci.*, *63*, 1587–1604.

Mu, M., W. S. Duan, and B. Wang (2003), Conditional nonlinear optimal perturbation and its applications, *Nonlinear Process. Geophys.*, *10*, 493–501.

Mu, M., L. Sun, and D. A. Henk (2004), The sensitivity and stability of the ocean's thermocline circulation to finite amplitude freshwater perturbations, *J. Phys. Oceanogr.*, *34*, 2305–2315.

Neelin, J. D., D. S. Battisti, A. C. Hirst, F.-F. Jin, Y. Wakata, T. Yamagata, and S. E. Zebiak (1998), ENSO theory, *J. Geophys. Res.*, *103*, 14,262–14,290.

Oortwijin, J., and J. Barkmeijer (1995), Perturbations that optimally trigger weather regimes, *J. Atmos. Sci.*, *52*, 3932–3944.

Palmer, T. N., et al. (2004), Development of a European multimodel ensemble system for seasonal-to-interannual prediction (DEMETER), *Bull. Am. Meteorol. Soc.*, *85*, 853–872.

Philander, S. G. (1990), El Nino, La Nina, and the Southern Oscillation, 289 pp., Elsevier, New York.

Picaut, J., and T. Delcroix (1995), Equatorial wave sequence associated with the warm pool displacement during the 1986–1989 El Nino and La Nina, *J. Geophys. Res.*, *100*, 18398–18408.

Powell, M. J. D. (1982), VMCWD: A FORTRAN subroutine for constrained optimization, DAMTP Report 1982/NA4, University of Cambridge, England.

Saha, S., et al. (2006), The NCEP Climate Forecast System, *J. Climate*, *19*, 3483–3517.

Samelson, R. G., and E. Tziperman (2001), Instability of the chaotic ENSO: The growth-phase predictability barrier, *J. Atmos. Sci.*, *58*, 3613–3625.

Suarez, M. J., and P. S. Schopf (1988), A delayed action oscillator for ENSO, *J. Atmos. Sci.*, *45*, 3283–3287.

Sun, L., M. Mu, D. J. Sun, and X. Y. Yin (2005), Passive mechanism of decadal variation of thermohaline circulation, *J. Geophys. Res.*, *110*, C07025, doi:10.1029/2005JC002897.

Tang, Y. M., R. Kleeman, A. M. Moore, and A. Weaver (2003), The use of ocean reanalysis products to initialize ENSO predictions, *Geophys. Res. Lett.*, *30*(13), 1694, doi:10.1029/2003GL017664.

Thompson, C. J. (1998), Initial conditions for optimal growth in a coupled ocean-atmosphere model of ENSO, *J. Atmos. Sci.*, *55*, 537–557.

van Oldenborgh, G. J., G. Burgers, S. Venzke, and C. Eckert (1999), Tracking down the ENSO oscillator with an adjoint OGCM, *Mon. Weather Rev.*, *127*, 1477–1495.

van Oldenborgh, G. J., M. A. Balmaseda, L. Ferranti, T. N. Stockdale, and D. L. T. Anderson (2005), Evaluation of atmospheric fields from the ECMWF seasonal forecasts over a 15-year period, *J. Climate*, *18*, 3250–3269.

Walker, G. T. (1924), Correlation in seasonal variations of weather IX: A further study of world weather, *Mem. Indian Meteorol. Dep.*, *24*, 275–332.

Wang, C. Z. (2001), A unified oscillator model for the El Nino-Southern Oscillation, *J. Climate*, *24*, 98–115.

Wang, B., and Z. Fang (1996), Chaotic oscillation of tropical climate: A dynamic system theory for ENSO, *J. Atmos. Sci.*, *53*, 2786–2802.

Wang, B., T. Li, and P. Chang (1995), An intermediate model of the tropical Pacific Ocean, *J. Phys. Oceanogr.*, *25*, 1599–1616.

Wang, B., A. Barcilon, and Z. Fang (1999), Stochastic dynamics of El Nino-Southern Oscillation, *J. Atmos. Sci.*, *56*, 5–23.

Webster, P. J. (1995), The annual cycle and the predictability of the tropical coupled ocean-atmosphere system, *Meteorol. Atmos. Phys.*, *56*, 33–55.

Webster, P. J., and S. Yang (1992), Monsoon and ENSO: Selectively interactive systems, *Q. J. R. Meteorol. Soc.*, *118*, 877–926.

Xue, Y., M. A. Cane, and S. E. Zebaik (1997), Predictability of a coupled model of ENSO using singular vector analysis. Part I: Optimal growth in seasonal background and ENSO cycles, *Mon. Weather Rev.*, *125*, 2043–2056.

Zavala-Garay, J., A.M. Moore, and R. Kleeman (2004), Influence of stochastic forcing on ENSO prediction, *J. Geophys. Res.*, *109*, C11007, doi:10.1029/2004JC002406.

Zebiak, S. E., and A. Cane (1987), A model El Nino-Southern Oscillation, *Mon. Weather Rev.*, *115*, 2262–2278.

W. Duan and M. Mu, LASG, Institute of Atmospheric Physics, Chinese Academy of Sciences, Beijing 100029, China. (mumu@lasg.iap.ac.cn)

B. Wang, Department of Meteorology, School of Ocean and Earth Science and Technology, University of Hawaii, Honolulu, HI, USA.